Accepted Manuscript

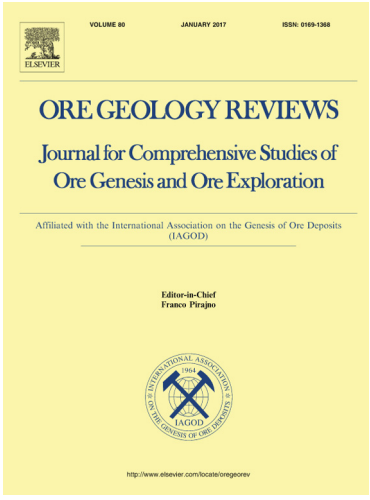

Neotectonics, remote sensing and erosion cut of ore-controlling structures of the Mnogovershinnoe gold-silver deposit (Khabarovsk Krai, Russian Far East)

Sergei Shevyrev

PII: S0169-1368(17)30898-3
DOI: https://doi.org/10.1016/j.oregeorev.2018.11.016
Reference: OREGEO 2743

To appear in: *Ore Geology Reviews*

Received Date: 20 November 2017
Revised Date: 7 November 2018
Accepted Date: 17 November 2018

Please cite this article as: S. Shevyrev, Neotectonics, remote sensing and erosion cut of ore-controlling structures of the Mnogovershinnoe gold-silver deposit (Khabarovsk Krai, Russian Far East), *Ore Geology Reviews* (2018), doi: https://doi.org/10.1016/j.oregeorev.2018.11.016

Neotectonics, remote sensing and erosion cut of ore-controlling structures of the Mnogovershinnoe gold-silver deposit (Khabarovsk Krai, Russian Far East)

Sergei Shevyrev, Far Eastern Federal University, Far East Geological Institute of the Far Eastern Branch of the Russian Academy of Sciences, Vladivostok, Russian Federation

Corresponding author: shevirev@mail.ru

Abstract

The Mnogovershinnoe epithermal gold-silver deposit is located on the northern part of the East Sikhote-Alin magmatic belt of Northeast Russia. This deposit is related to the intrusion of a large multiphase Paleogene Bekchiul granitoid pluton. The research area underwent several episodes of intrusion magmatism, volcanism and isostatic uplifting because of its location at the junction point of large tectonic structures of Asia. The integration of in situ observations, geological mapping data, analysis of the Landsat 8 images and digital elevation data provides insights into the Meso-Cenozoic evolution of the Bekchiul magmatic center. Events in the Neogene-Quaternary were sufficiently restored by detecting areas with anomalous differences from the base level surfaces for the second- and third-order streams and numerical modeling. The anomalous values of the base levels difference far exceed the amplitude of sea level regression during the Neo-Pleistocene. The proposed methodological approach considered isostatic uplifting and sustaining activity as guiding factors in the development of the Bekchiul volcano-plutonic center.

Keywords: remote sensing of the Earth, gold deposits, neotectonics, erosion level, numerical modeling, isostasy, Sikhote-Alin folded belt

1. Introduction

The Sikhote-Alin folded belt is a polygenic tectonic structure south of the Russian Far East. This belt occupies a considerable part of the Khabarovsk Krai and most of Primorye and is bounded by the Sea of Japan on the southeast side and the Sea of Okhotsk on the north side (Fig. 1). Tectonic activity in this belt is governed by an interaction of the Pacific plate with the eastern margin of the Asian continent, where a geophysical study revealed a stagnant oceanic slab in the mantle transitional zone (Zhao et al., 2010; Maruyama et al., 2007). Sikhote-Alin was formed during the Last Cretaceous and underwent alternating episodes of intrusive magmatism and volcanism.

The southern portion of the Russian Far East has native gold, gold-silver and complex precious metals deposits in the Lower Amur (Cretaceous-Paleogene) ore region in Khabarovsk Krai and the Kema (Paleocene) ore region in Primorye. The Lower Amur region occupies the northern part of the East-Sikhote-Alin volcanic-plutonic belt (ESAVPB) and is endowed with abundant Au-Ag deposits.

The Kema ore region is associated with the eastern part of the ESAVPB, where the Kema island-arc terrane is intruded and overlain by volcano-magmatic rocks. This ore region unites a gold-silver epithermal vein and Cu-Mo (±Au, Ag) porphyry, Cu (±Au) porphyry, and Mo (±W, Sn, Bi) porphyry deposits in the considered area.

The Mnogovershinnoe epithermal gold-silver mineralization of the Lower Amur ore region is one of the largest complex precious metal deposits in the Russian southeast with a remaining endowment of more than 19.8 t Au (Mnogovershinnoe…, 2017). The origin and geological history of this mineralization is the subject of particular interest. The deposit is located in the

northwestern sector of the large (approximately 520 km^2) Bekchiul volcano-plutonic center surrounded by late Cenozoic paleovolcanic structures and includes several elongated vein-metasomatic ore zones of considerable thickness with different degrees of erosion (Utkin, 1999).

The area adjacent to the Bekchiul pluton is scarcely populated and settled predominantly by gold prospectors and native tribes. Only several years ago, a road finally connected Mnogovershinnoe with the rest of the territory. Thus, state geological mapping, mineral prospecting and exploration remain the main sources of geological, geomorphologic and stratigraphic information. The examination of ore textures revealed several episodes of pulsating stretching, while a detailed study of the magmatic complexes, radiometric dating, numerical geodynamic modeling and computation of the erosion network's peculiarities revealed anomalous elevations related to the Bekchiul tectono-magmatic center.

The hydrothermal system of the Mnogovershinnoe deposit is considered to be polygenic. At an early stage, the hydrothermal fluids migrated from the cooling periphery of the volcanic-plutonic complex along fractures. During the cooling of magmatic system, the outflowing fluids mixed with the meteoric ones, but new portions of intruded magma rejuvenated the hydrothermal system and replenished the fluid pressure (Fatyanov et al., 2009; Khomich et al., 2017).

The goals of this study include detecting Neotectonic uplifts related to the arguable isostatic rise of the Meso-Cenozoic Bekchiul volcano-plutonic center and reconstruction of the regional geological history according to the sequence of ore generating hydrothermal processes, sequence of magmatic intrusions, modeling of isostatic floating and results of remote sensing data analysis.

2. Geological settings

The research area is located at the junction point of large structural elements, namely, the East Sikhote-Alin folded belt, Amur-Okhotsk fold system and Okhotsk-Chukotka volcanic belt (Fig. 1). The area is the peripheral projection of the stagnant mantle slab over which the world-class Aldan, Balei (Russia), Zhao-E (China) deposits along with numerous gold deposits with fewer resources were revealed. This fact agrees with the theory of the origin of ore deposits associated with mantle upwelling (Zhang et al., 2013).

The Mnogovershinnoe deposit is situated in the Lower Amur ore district, which is the northern segment of the East-Sikhote-Alin continental marginal orogen. The deposit is related to the Ula volcanic-plutonic structure located at the northwest flank of the Bekchiul volcano-plutonic center (Utkin, 1999). The Ula structure occupies a zone of minimum gravity and contrast magnetic fields (Khanchuk, 1993).

The basement of the Ula structure is composed of terrigenous rocks of the Jurassic-Lower Cretaceous age: sandstone, argillite and siltstone (Fig. 1). The volcanic assemblage consists of Paleocene clastic lavas and subvolcanic rocks, andesite and andesite-dacite. Both of these structural levels are intruded by the exposed Bekchiul granite massif, which has a total extent area of approximately 520 km^2. The Mnogovershinnoe deposit belongs to the northwestern flank of the Bekchiul massif (Khanchuk, 2006).

Magmatic rocks of the Bekchiul massif are divided into two paragenetic associations according to the order of intrusion. The early association comprises poorly differentiated andesite-granodiorite of normal alkalinity, whereas the later one includes highly differentiated subalkaline monzo-granodiorite and granite. The gold-silver mineralization is spatially related to the Ula andesitic volcano (Fig. 1, letter “U” in the circle). The Ula volcano is one of the largest subdominant volcanic structures of the Bekchiul massif and is expressed as a local depression

along the northwestern contact of the Bekchiul massif. The underlying Upper Jurassic – Lower Cretaceous sedimentary rocks of the basement are deformed into linear folds of a northeastern strike. The volcanic facies are hydrothermally altered with different intensity (Fig. 2) (Fatyanov and Khomich, 1997). Gold-silver mineralization of the Mnogovershinnoe deposit is concentrated in the long (up to 10 km) and thick (up to 100 m) vein-metasomatic zones traced to a depth of 600 m in the rocks of the volcanic assemblage and basement.

The NE-trending ore-controlling faults were inherited from the folded deformations of the terrigenous basement (Fatyanov and Khomich, 1997). These faults are responsible for the step-like block dislocations of the deposit. The thickness of the volcanic cover increases as the distance from the Bekchiul massif increases, which may explain the higher degree of erosion of the ore zones near the Bekchiul massif (Fig. 3).

The successive stages of the Bekchiul massif formation predefined the appearance of the vein-metasomatic zones of different genesis in the Mnogovershinnoe ore field. There are different types of hydrothermally altered rocks both ore-bearing and barren (Fatyanov and Khomich, 1997):

- metasomatite of acid leaching, which has northeast oriented bodies;
- quartz veins related to an extension of the northeastward faults;
- breccia zones with quartz, adularia-quartz and carbonate-quartz cement;
- ore-bearing skarn-like metasomatite related to subalkaline intrusions;
- ore-bearing pre- and postskarn carbonate;
- tourmaline-quartz veinlets related to an intrusion of monzonite granite.

The mineralization of commercial interest is localized in three basic zones: Glavnaya, Promezhutochnaya and Medvezh'ya. The mineral composition of these zones comprises quartz, adularia-quartz with sericite, chlorite and carbonate. Sulfide minerals are abundant (up to 0.5-3%) with a predominance of pyrite, chalcopyrite, galena, sphalerite, pyrrhotite, and arsenopyrite. Sulfosalt minerals, telluride (hessite, petzite), and disseminated native gold play a subordinate role.

Tellurobismuthite, altaite, scheelite, selenide (naumannite), telluroselenides of silver and galena-clausthalite occur rarely. Post-ore skarn-like metasomatite contains magnetite and hematite (Fatyanov et al., 2007; Khomich et al., 2017).

The set of in situ sampling (Fig. 4) allows reconstruction of the staging of the ore deposition and mineralization process. In addition to the pyrite-chalcopyrite ores (Fig. 4E), several generations of quartz are presented as the breccia cement for early vein minerals (Fig. 4A) and volcanic-sedimentary country rocks (Fig. 4B). Wollastonite and bustamite substitute the carbonates precipitated along the main stage of the ore deposition (Fig. 4C-D). Pleistocene basalts intrude ore bodies and contain striped ores as xenoliths (Fig. 4E).

Dislocations in hydrothermally altered rocks keep the evolution record of the Bekchiul massif. In situ sampling of the streaks from the Mnogovershinnoe deposit shows relationships between the appearances of early and later minerals (Fig. 5). As seen in the figure, the area has several generations of fractures impregnated by the minerals: a fractured rock mass of epidote, actinolite and diopside was injected by veins of nephritis and tremolite (Fig. 5A), veins of bustamite and rhodonite with quartz fill the breccia of early quartz (Fig. 5E), and quartz-wollastonite veins compose early quartz breccia (Fig. 5F). Staging seen in these samples suggests tectonic control of the associated hydrothermal regime when the previously existing fractures were rejuvenated and expanded, and then precipitation of the new minerals occurred.

Previous research (Khomich et al., 2017) distinguished main gold ore stage (I) and two post-ore stages, skarn-hydrothermal (II) and late hydrothermal (III). These stages are characterized by mineral associations (1-10), where "rock-forming", "main", "considerable" and "accessory" mineral classes are subdivided (Fig. 6).

Successive generations of mineralized veins show evidence for the supposed pulsating manner of the tension stress field, where magmatic and/or tectonic factors opened fractures and changed the pressure regime of migrating fluids. Isotope dating of Cretaceous-Paleogene intrusion phases (Khomich, 2017; Kaydalov et al., 2001) and base surface analysis of the Neogene-Quarternary dynamics helped to reconstruct the tectonomagmatic evolution of the Bekchiul massif.

Prospecting of the northwestern flank of the Bekchiul volcanic-plutonic structure promoted knowledge of the tectonic settings and ore genesis. Native gold content of other areas at the same time has not been thoroughly elucidated to date, although rivers of the territory are characterized by a wide development of placer deposits.

The field mapping and observations have shown that rivers of the southwestern part of the study area fall into Chlya and Orel lakes, whereas others empty into Sakhalin Bay of the Sea of Okhotsk. The Malakhta, Bekchi, Ul, and Tyvlinka rivers stand out among others. These rivers form a typically dendritic branched drainage pattern of the Neogene age. Based on current concepts, the Pliocene-Early Neopleistocene peneplain and weathering crust were found to be overlain by Early and Middle Neopleistocene alluvium on the watersheds of the Tyvlinka, Syvuk and Vynga rivers (Kaydalov et al., 2001).

Weathering crust of the Pliocene-Early Neopleistocene is widespread across the Sivuk-Tyvlinka interfluves (Kaydalov et al., 2001). The crust consists of a clay

with a relic structure of the parent rocks. A crust is developed over the sedimentary, volcanogenic and intrusive rocks. Composition of the weathering crust depends on the mineralogy and structure of the underlying rocks. The total thickness of this crust is up to several tens of meters on the magmatic rocks, whereas on the sedimentary rocks, including the Miocene, it has thickness up to 5-7 m. The appearance of a weathering crust of the Pliocene-Lower Neopleistocene age arguably marks the absence of active tectonics during the Pliocene-Lower Neopleistocene and a hiatus in the sedimentation (Kaydalov et al., 2001).

The remains of peneplain were detected at heights of 20 to 80 m (Kaydalov et al., 2001). Similar to the other main rivers of the area, the Tyvlinka river has the highest, i.e., a fourth order, stream order or Strahler number (Strahler, 1957) in the region. This river allowed authors of the state geological map to consider the Neogene period as a time of relatively calm tectonics after the Eocene-Oligocene basaltic eruptions (Krasny et al., 1999). Networks of tributaries (streams of lesser order) have formed since the Oligocene and have recorded events of geological history that affected local and global base levels of erosion.

A drilling cross-section through the Sivuk-Tyvlinka interfluve showed relations between the Oligocene, Miocene and Neopleistocene deposits on the area (Fig. 7). The Miocene lacustrine and alluvial deposits were accumulated on the eroded surface of the Albian-Cenomanian deposits and Oligocene basalts. The erosion network in its present state was formed after the Middle Neopleistocene, which is indicated by the weathering crust eroded by the Tyvlinka River of 3-4 Strahler number.

The global base level of erosion was affected by glacial fluctuations of the sea level. Local changes in the erosion regime conformed to grabenization or uplifting, forming of volcanic centers, etc. (Kaydalov et al., 2017).

Events of post-Eocene time obtained from the geological mapping and prospective drilling are generalized in Table 1. Miocene deposits of the Pre-Pleistocene erosional network were dated by spores and pollen, while the rest of the aging was determined by efforts of a mapping survey with radiocarbon and thermoluminescence dating (Kaydalov et al., 2017).

Table 1. Late Cenozoic events that affected the vicinity of the Bekchiul volcano-magmatic center in Post-Oligocene history

Number	Age, kyr	Age name	Event	Evidences
1	16,5-8	Holocene	Present-time transgression	Recent marine, alluvial and lacustrine sediments of the area
2	16.5-26.5	Upper Pleistocene	Sartan glacial regression	Reduction of the sea and erosion levels up to 120 m, erosion of land alluvial deposits, alluvial deposition on the shelf
3	26,5-37,5	Upper Pleistocene	2nd stage, Kazantsev transgression	Clay and sand of sea terrace
4	38.1-41.3	Upper Pleistocene	1st stage, Karginskoye transgression	First sea terrace and alluvial sea terrace, sands and aleurite
5	60–74	Upper Pleistocene	Zyryan regression	Reduction of the sea and erosion levels up to 120 m, erosion of land alluvial deposits, alluvial deposition on the shelf
6	?	Pre-Middle	Forming of	Forming of weathering

		Pleistocene	weathering crust	crust over the Miocene lacustrine-alluvial deposits
7	?	Miocene	Forming of ancient river network	Erosion of Mesozoic sedimentary rocks and Oligocene basalts; accumulation of continental strata

Active behavior of the Bekchiul volcanic-plutonic center for the post Oligocene time could be due to the following facts:

- In contrast to the surrounding peneplain, the Bekchiul structure has middle (10-20º) and steep slope angles (20-30º) and an intensively dissected relief (1.2-1.8 km/km^2);
- With the Bekchiul center, the watersheds are straight and convex, and talus deposits are abundant in the lower parts, whereas the upper parts are jagged with frequent erosional remnants without accumulation deposits;
- Despite volcanic activity of the Bekchiul ceasing in the Oligocene, the massif considerably exceeds the surrounding peneplain and is even eroded to its core parts. The overlaying deposits remain at the periphery and are uninvolved with uplifting.

3. Research methodology

3.1. Base level surface analysis with SRTM data

The erosional network records the information about the base erosional levels of the area and their changes according to fluctuations of the global sea level as well as grabenization and orogenic movements. The signs including network branching, number of tributaries and their hierarchy, their planar pattern,

transversal profile of the valley and terrace number contain the succession of events from the very appearance of the river network. Strahler (1957) and Horton (1945) offered an approach for computing the order of streams. The elder rivers, which drain to the sea, have the highest Strahler number in the area; recent streams have a smaller number, while modern ones have the smallest number. Elder rivers were formed due to major tectonic and/or climatic changes of the area, which restarted the sedimentary cycle.

According to Strahler (1957), a first order stream has no tributaries, as opposed to higher order streams. The major rivers of the area under study are the fourth–order streams, and consequently, their tributaries are third-order streams.

The base level surface, which was computed for the streams of the same order, reflects the relative position of the erosional basis at the time of their development. A relative decrease of the erosional base or local uplift provokes incision of the tributaries and, as a result, increases the order of the main streams. Whereas global changes in sea level produce a simultaneous response of the whole stream network, local anomalous values of the difference between base surfaces usually have a lithological or tectonic background. Difference values reflect the amplitude of change in the erosional base. Uplifts are distinguished from erosional remnants, which are specific to the rocks with a higher resistance to weathering, by the disagreement of local difference values with global changes of the erosion base level. In the case of remnants, the local values of the amplitude are usually less than that for active uplifts. Thus, the areas of uplifts can be determined by anomalous values of difference between the base level surfaces.

A method of base level surfaces (Philosofov, 1967; 1975) belongs to the classical methods of modern neotectonics. Application of GIS technologies can improve its precision and performance speed.

Base level surfaces were spline interpolated by the spline for the point data set, where each point has a value of discrete stream order height above sea level. In the classical implementation of this method, the point set is extracted from the intersection between isohypses and streams on the map. In digital cartography, the set is obtained from a raster SRTM overlay by the stream order binary map.

All computations for the map of neotectonic activity within the area according to base level surfaces were performed in MATLAB. Highlighting streams and determining their orders were performed by the MATLAB Topographic Toolbox (MTT) (Schwanghart, 2010). Application of this toolbox allowed rendering a map of stream orders (Fig. 8).

Base level surfaces (BLS) were computed by the Philosofov V.P. method (Philosofov, 1967; 1975), which was updated for processing the shuttle radar topography mapping digital elevation model (SRTM DEM). The streams of a given order were considered as a mask for extraction of the DEM pixels with riverbed altitudes to compose a sparse matrix. The nonzero elements of the matrix were used for interpolation of the base surfaces. The first-order streams were ignored because their base surface approximates the contemporary relief. At the same time, the forth-order streams have the most ancient base surfaces, which reflect changes in the global erosional base and correspond to the planetary processes.

Thus, the second- and third-order streams are suitable for evaluation of amplitudes of the Neogene-Quaternary tectonic processes. Figure 9 (Fig. 9) shows the extracted second- and third-order streams over the DEM, their base level surfaces and difference between them. This image demonstrates stages of the base level surface computing:

- Separation of streams of 2nd order (Fig. 9a);
- Separation of streams of 3rd order (Fig. 9b);

- Selection of DEM heights overlain by points of second and third order streams;
- Interpolation of base level surfaces for second (BLS2) and third (BLS3) levels of streams (Fig. 9c-e);
- Computing difference surface (BLDS23) for the previous two values (Fig. 9f).

The analysis of base erosional surfaces of the second- and third-order streams (BLS2 and BLS3, respectively) and the base level difference (BLS2-BLS3 or BLDS23) was implemented for an assessment of the relief-forming endogenous processes. The Neogene-Quaternary tectonic activity of the Sikhote-Alin can be considered to be inherited from the continuous subduction of the Pacific plate under the East Asian margin.

BLDS23 reflects to what extent the local base level of erosion traveled from the time of the second-order stream's formation until the time of the third-order stream's origin. A comparison with underlying rocks provides information regarding the nature of these zones (Fig. 10). Figure 10c shows a notable depression of BLDS23 in the central part of the Bekchiul pluton, whereas the northwestern part (from the Ula volcanic center to the sea coast) is notably uplifted. Volcanic centers of the Oligocene are expressed similarly. The northwestern part of the area contains a positive BLDS23 anomaly over the Cretaceous granites, which are not related to the Bekchiul massif.

3.2. Fracture tectonics analysis with remote sensing data

Because the southern territories of the Russian Far East have a thick layer of soils and dense forest cover, which impede direct geological observations, interpretation of the remote sensing data is important. The fracture pattern detected in Landsat imagery can be one of two types: line elements and lineaments.

Analysis of the fracture pattern comprises automatic image processing technologies: the Canny algorithm for image binarization and the linear Hough transform for detecting linear features. Detected lines could be combined based on their collinearity to derive lineaments, which are assumed to be tectonic disjunctives. The applicability of these algorithms for the fracture pattern analysis was tested by Healy et al. (2017) and Hashim et al. (2012), as well as other authors. These algorithms serve the role of feature recognition in LEFA (lineament extraction fracture analysis) software; the MATLAB-based scripting toolset is used for linear feature detection and exporting into the ESRI Shape format (Shevyrev, 2018).

Lineaments extracted from the tiled Landsat 8 images (band 7; acquisition dates: 2016-08-25, 2015-08-02) formed a system of northeastern and northwestern directions, which correspond to principal trending of first- and second-order faults of the East Sikhote-Alin folded belt (Fig. 11). After automated extraction, the lineaments were resampled by hand to remove overlaps and features of supposed nontectonic nature. The faults' intersection over the core part of the Bekchiul massif is remarkable. This radial pattern may be evidence of the local uplift in this zone. Because lineaments are expressed in the contemporary post-Miocene relief, they are probably from the post-Miocene age or were activated in post-Miocene time.

3.3. Numerical modeling of the rheological floating

Reconstruction of the Mnogovershinnoe ore field formation, including an appearance of the thermal field, intrusion episodes and interaction between the hydrothermal and meteoric waters, was proposed in a recent paper (Khomich et al., 2017). However, the previous model did not explain the nonuniform erosional cut of the ore zones, denudation of the deepest parts of the Bekchiul till and anomalies

of base erosion surfaces. The leucocratic core of the Bekchiul massif coincides with the contrast minimum of the gravity field (<–10 mGal) (Petryschevsky, 1984). These facts suggest the applicability of rheological (viscous) models for tectonic reconstruction. To explain probable isostatic uplift of the less dense quartz core of the Bekchiul massif, a semiquantitative 2D MATLAB model of a floating block (from (Gerya, 2010) with changes) was applied. This model solves the 2D Stokes continuity and advection equations using the finite differences and marker-in-cell technique. The model simulated the interaction between the media (50x50 km) and block (10x10 km), while considering their density and viscosity. An abundance of quartz in the subalkaline granites of the 4th phase and surrounding rocks creates a difference in density between the core and peripheral parts of the massif.

The values of the rock density for the model input data were taken from Turcotte and Schubert (2014) Appendix B.5 (Properties of Rocks). The dynamic viscosity of granite in this reference was determined by Japanese researchers Kumagai Naoichi, Sasajima Sadao, and Ito Hidebumi (1978) during a long-term experiment to vary between 3e19 – 6e19 Pa·s. Thus, the model input parameters are:

- Densities 2700 kg·m^{-3} for the granodiorite (media) and 2650 kg·m^{-3} for the subalkaline granite (buoyant block);
- Viscosity 4.5e19 Pa·s both for the media and block.

Execution of the model produced the graphic output shown in Fig. 12. For 30 steps of the model work (approximately 4.2 Myr), the block rose 11.9 km, which corresponds to a mean velocity of 2.83 mm/year. This continuous isostatic rise after the intrusion of critical amounts of subalkaline granite magma can explain the profound erosion of the Bekchiul massif, denudation of the overlaying Cretaceous and Oligocene vulcanites, differentiated erosion of the ore bodies in the Mnogovershinnoe deposit and revealed evidence of neotectonic activity. In fact, the leucocratic core of the Bekchiul massif (subalkaline granite of the fourth phase)

surrounded by the denser granodiorite creates a critical difference in density, thereby leading to core upthrust. The protrusion of the country rocks by the leucocratic core forms an uplift in the peripheral parts of the massif followed by local descending of the erosional base and relative elevations of watersheds over the thalwegs.

The neotectonic processes, which contributed to the formation of the Bekchiul massifs relief, were followed by strain accumulation. The succeeded release of strain is reflected in the contemporary seismicity of the area. In fact, the Bekchiul massif and its vicinity are distinguished by an occurrence of recent (1962–2004) shallow-focus (< 10 km) earthquakes of small magnitude (< 4.9) (Khanchuk, 2006; Tikhonov and Lomtev, 2014).

4. Evolution of the Bekchiul volcanic-plutonic center

Reconstruction of the sequential events in the history of the Bekchiul tectonomagmatic center, as well as detection of the residual Neogene-Quarternary uplifts, requires a synthesis of absolute dating, field observations, in situ sampling and numerical computer modeling. In addition to the remote sensing data analysis, we summarized all affordable factual evidence that indicate the past geodynamic regimes of the Bekchiul.

Analysis of streams and reconstruction of their formation regimes allows the detection of local Past-Miocene-Quaternary uplifts, which reflect regional tectonic processes.

The mapping of base level surfaces revealed zones of local tectonic movements (Fig. 13). A comparison with the geological background showed a coincidence of positive difference anomalies with the outer part of the Bekchiul massif, primarily composed of quartz diorite and montzodiorite. There are peak

values that reach 233 m and less contrast local maxima up to 30 m. By considering the inevitable erosion of the massif in the later Cenozoic, we can assume that the relative descent of the erosion base was greater than 233 meters. However, mapping of the Sakhalin Gulf confirms the Sea of Okhotsk regression until the 120-m isobath in the Zyryan (60–74 kyr) and Sartan (16.5– 26.5 kyr) glaciations of the Quaternary (Galanin, 2012; Kaydalov, 2001).

The rendered images of BLS2, BLS3 and BLDS23 have been compared with the geological structure of the area and episodes of sea level regression taken from the Sakhalin Gulf maps (Kaydalov, 2001). The development of a generalized scheme of the area also demanded data of fracture tectonics, which were acquired from processing the Landsat 8 imagery in the LEFA MATLAB software (Shevyrev, 2017; 2018). A comparison of detected lineaments with the supposed elevated areas allowed detection of tectonic uplifts from erosional remnants (Fig. 13).

Areas under the influence of global changes in the erosional base include the zones of active local uplifts (BLDS23>100 m) of smaller size. Erosional remnants outside the Bekchiul area (BLDS23<100) are related to the Cretaceous and Paleogene intrusions. Marginal parts of the Bekchiul massif and peripheral volcanic centers trace a zone of uplifts with amplitudes greater than 260 m. A system of radial faults detected by remote sensing in the southwest of the subalkaline core intersects this zone. A reconstruction of tectonic events that led to the described structure of the Bekchiul massif is considered below.

The figure (Fig. 14) contains an evolved and augmented model with principles primarily proposed by Igor Fatyanov for pre-ore regime and ore genesis only (Khomich et al., 2017) of the Bekchiul center. The history of recorded events was extended up to the Oligocene by implementation of supplementary radiometric dating, drilling of the Neogene-Quaternary strata and base surface analysis.

Summing up the facts above, we can reconstruct the Meso-Cenozoic evolution of the Bekchiul magmatic center. There are 8 stages embracing events of magma emplacement in the Cretaceous-Paleocene, and two episodes of volcanism and solid-state buoyancy of the massif core resulting from a density difference. The evolution of the Bekchiul volcano-magmatic center includes episodes of pulsating expansion of fractures both of "magmatic" and "tectonic" origin.

Stage 1 (Fig. 14) describes the existence of the thermal field on the area. Researchers (Khomich and Boriskina, s2014ab; Khomich et al., 2017) have seen the leading role in high thermal inflow in the tectonic position of the Bekchiul center on the periphery of the stagnant mantle slab over the paleo-transform fault. This zone was permeable for magmas as well as migrating fluids, so the heated meteoric waters formed a pre-ore hydrothermal system in the area.

Stages 2-5 comprise andesite volcanism and a sequence of granitic intrusions phases with increasing silica content.

Stage 6 started when the amount of acidic granites of the Bekchiul core exceeded the limit necessary for buoyant forces to dominate. Uplift was followed by erosion of the Bekchiul dome; hence, only the Upper Cretaceous andesites remained in the peripheral parts.

Stage 7 depicts the effusion of Oligocene basalts, which intruded into ore bodies of the Mnogovershinnoe deposit (Fig. 4F) and covered at least part of Bekchiul massif and coastal peneplain.

Stage 8 comprises the time span after the Oligocene basaltic volcanism (24.5±2.0 Ma) to the Holocene. A prospective drilling profile through the Sivuk-Tyvlinka watershed demonstrated the presence of an extinct Miocene erosion network with its sediments overlain both over the Oligocene basalts and Cretaceous strata. Drilling discovered weathered pebbles with a blue clay, which marks a hiatus in sedimentation in the Miocene coarse-grained layers up to 50 m

thick. The Middle-Upper Neopleistocene deposits fill present-day valleys. Holocene peat and pebbles overlay the watersheds of the coastal plains.

5. Discussion

The evolution of the research area was affected by three factors: (1) glacial changes of the sea level, (2) pulses related to magma intrusion into the underlying rocks or lava flooding of a pre-existing relief and (3) rheological floating-up of the less dense acidic Bekchiul massifs core.

In contemporary research, one of these factors is considered to be the leading factor because of its critical role.

Glacial changes, including fluctuations of the sea level in the Quaternary, have appeared globally, while the isostatic postglacial uplifting of the dry-land is only a regional influence, which is indicated in numerous studies (for example, Turcotte and Schubert, 2014; Siddall et al., 2003; Schofield, 1964; Firth and Stewart, 2000; Smith et al., 2017; Stockamp et al., 2016; and others). Research of isostatic postglacial floating-up of ancient glacial centers of Scandinavia revealed an uplifting velocity of approximately 2 mm/year for marine terraces of Östergransholm, Eastern Gotland, Sweden (Turcotte and Schubert, 2014). This velocity of postglacial compensation is comparable with our numerically simulated velocity of 2.83 mm/year. Sea level fluctuations changed the contours of shore lines, formed marine terraces, closed or opened straits and, consequently, affected river networks (Park et al., 2000; Edwards and Craven, 2017; Gaidzik and Ramírez-Herrera, 2017; Kiden and Törnqvist, 1998).

Contemporary views of the response of erosion networks to the uplifting were proven experimentally (Lague et al., 2003). In the case of a glacial load and/or sea level changes, the amplitude of the relative changes in elevation, and

consequently, erosion or accumulation of relief is generally slightly higher than one hundred meters. However, a decrease in the sea level during the Pleistocene formed the extensive Beringia dry land, which connected North America and Asia before it was flooded 11 Kyr ago according to lithological and geophysical data (Jakobsson, 2017).

Biostratigraphic methods are also applicable in neotectonic research. A study of recent elevations in the Mediterranean mobile belt revealed adjacent area uplifting velocities of Antakya Graben by dating marine terraces with mollusk fauna (Tari et al., 2018). Taking into account global sea level oscillations allowed the detection of velocities of regional uplifts from ~ 0.43 ± 0.11 mm/yr to 2.08 ± 0.70 mm/yr for Antakya Graben's vicinity (Tari et al., 2018).

An endogenous factor of relief evolution is generally considered as leading for large active Meso-Cenozoic tectonic structures of different areas (for example, Miller and Becker, 2014; Khanchuk, 2006). Researchers of tectonic (crustal) and plume (mantle) processes generally believe that relief forms produced by plumes are characterized by axial symmetry and longwave topography, whereas a crustal tectonic relief is generally asymmetric and corresponds to shortwave topography (Burov and Gerya, 2014; Hager et al., 1985; van der Hilst et al., 1997).

The plume process is immediately related to the sculpturing of the divergence zone including the formation of the rift valleys and step faults series (van Wijk et al., 2018; Burov, Gerya, 2014). Volcanologists detect local crustal deformations, which have a relief expression and can indicate awakening of volcanoes, as well as accompany eruptions and volcanic elevations (Peltier, 2016; Okada, 1985). Similar processes are abundant over the subduction zone of the Western Pacific, where they are the subject of a detailed study. Analysis of the geochemical, isotope and petrological characteristics of magmatic rocks allowed the assessment of the geodynamic regime of the contemporary and Neogene-

Pleistocene stratovolcanoes of the Kuril-Kamchatka island arc system (Avdeiko et al., 2007). In Vietnam, Thailand, Cambodia and Laos, Neogene-Pleistocene basaltic plateaus occupy more than 70,000 km^2. Geochemical data indicate their correspondence with the collision between south Asia and fragments of Gondwana (Hoang et al., 2013).

Several studies emphasize the necessity of a synthesis between modern tectonic paradigms and the theory of Pleistocene climatic changes, which takes into account changes in sea level (Cloetingh and Haq, 2015; Weil-Accardo, 2016). Quantitative features of the neotectonic movements were revealed by studying terraces (Lave and Avouac, 2001; Šujan and Rybár, 2014; Dai et al., 2005 и другие). It was shown that growth of the Nepal Himalayas is indicated by the simultaneous incision of a river network with activation of the slope processes (Lave and Avouac, 2001).

Magnetostratigraphic research of Cenozoic alluvial sediments allowed dating of recent uplifts of the Tibetan plateau associated with a collisional regime (Dai et al., 2005). Recent and ancient deformations could also be detected using satellite radar interferrometric observations (Trasatti, 2018; Guo et al., 2017).

Consequently, the duration and velocity of neotectonic movements could be revealed with bio, magnetostratigraphic and instrumental methods including satellite radar observations. The method of base erosional surfaces, which was implemented in our research for detection of the uplifts, embraces the time interval since the contemporary erosional network development starts. Meanwhile, the velocity of uplifting could be determined using numerical modeling.

The updated method of the base level surface analysis could be a source of information for the reconstruction of the formation of ore deposits when it is joined with contemporary remote sensing technologies. The method reveals specifics of the post-ore processes and the value of an erosional cut. A comparison of the

obtained data with the models of the ore field vertical zoning (e.g., (Sillitoe, 2010)) could assist in the assessment of its erosional level as well as its prospectivity for primary and placer deposits.

The geological history of the Bekchiul massif was reconstructed since the Cretaceous. The intensity of the relief-forming processes was controlled by temporarily dominant factors: magma intrusion during active periods and gravitational floating in intervals of relative calm. The influence of the sea level changes was limited by the coastal areas and did not manifest in erosion of ore-controlling structures.

7. Conclusions

In our case study, an analysis of the base erosional surfaces and their difference revealed local uplifts that are associated with the core part of the Bekchiul massif. Such areas are of particular interest in terms of native and placer mineralizations.

In the northwestern part of the ESAVPB, these objects are related to the well-exposed, partially exposed and covered massifs or the eroded volcanic centers. All over the research area, detected uplifts are associated with gold placers; metasomatic mineralized zones could be discovered because of their erosion and accessibility for direct study. Our combined approach includes base surface analysis, field observations, mineralogical sampling and isotope dating. These data were used for the reconstruction of the Bekchiul volcanic-plutonic center and evolution of its relief since the Upper Cretaceous.

The results might be useful for geodynamic and ore prospectivity studies into the geological background of subduction boundaries. The considered Neogene-Quaternary processes, according to the age of the examined river

network, suggests Cenozoic continuing of Mesozoic tectonic activity of the ESAVPB north flank.

The approach and methodology described is recommended for neotectonic reconstruction and prospectivity assessment for native and placer precious metals deposits of large volcanic-plutonic centers.

Acknowledgements

The author deeply acknowledges Dr. Professor Khomich V.G. and Dr. Fatyanov, FEGI FEB RAS for the discussion. Advices of other colleagues and friends also contributed this work. Author would like to express special gratitude to anonymous reviewers for reading the manuscript and priceless recommendations.

References

Avdeiko, G.P., Savelyev, D.P., Palueva, A.A., Popruzhenko, S.V., 2007. Evolution of the Kurile-Kamchatkan Volcanic Arcs and Dynamics of the Kamchatka-Aleutian Junction. Volcanism and Subduction: The Kamchatka Region Geophysical Monograph Series, 172. Copyright American Geophysical Union. http://www.kscnet.ru/ivs/bibl/sotrudn/avdeiko/GM01015CH04.pdf

Burov, E., Gerya, T., 2014. Asymmetric three-dimensional topography over mantle plumes: Nature, v. 513, no. 7516, p. 85–89, https://doi.org/10.1038/nature13703.

Cloetingh S., Haq, B.U. Sea level change. Inherited landscapes and sea level change. January 2015Science 347(6220):1258375

Dai, S., Fang X., Song, C., Gao, J., Gao, D., LI., J., 2005. Early tectonic uplift of the northern Tibetan Plateau. Chinese Science Bulletin. 2005 Vol. 50 No. 15. P. 1642−1652.

Edwards, R., Craven, K., 2017. Relative Sea-Level Change Around the Irish Coast. In: Coxon, P., McCarron, S., Mitchell, F. (eds.) *Advances in Irish Quaternary Studies*. 181-215. Atlantis Press. https://doi.org/10.2991/978-94-6239-219-9

Fatyanov, I.I., Khomich, V.G., 1997. Bekchiul gold-bearing volcano-plutonic construction: magmatic associations, features of development, the scheme of formation (Lower Amur region). Tikhookeanskaya Geol. Vol. 16, pp. 32–44 (in Russian).

Fatyanov, I.I., Khomich, V.G., Boriskina, N.G., 2010. Hidden mineralogical and geochemical zonation of low-sulfide gold—silver mineralization (Mnogovershinnoe deposit, Lower Amur area). Dokl. Earth Sci. 435, 1456–1459. http://dx.doi.org/10.1134/S1028334X10110103.

Firth C.R., Stewart I.S., 2000. Postglacial tectonics of the Scottish glacio-isostatic uplift centre. Quaternary Science Reviews 19(14). P.1469-1493.

Gaidzik K., Ramírez-Herrera, M.T., 2017 Geomorphic indices and relative tectonic uplift in the Guerrero sector of the Mexican forearc. Geoscience Frontiers. Vol. 8. Issue 4. P. 885-902. https://doi.org/10.1016/j.gsf.2016.07.006

Galanin, A.A., 2012. Age of last glacial maximum of northeastern Asia. Earth's Cryosphere. Vol. XVI, №3, p. 39-52 (in Russian).

Gerya, Taras, 2010. Introduction to Numerical Geodynamic Modelling / Cambridge University Press. P. 292

Guo J., Xu, S., Fan H., 2017. Neotectonic interpretations and PS-InSAR monitoring of crustal deformations in the Fujian area of China. Open Geosciences. 9(1). P. 126-132.

Hager, B. H., Claytton, R. W., Richards, M. A., Comer, R. P., Dziewonski, A. M., 1985. Lower mantle heterogeneity, dynamic topography and the geoid. Nature 313, 541–545.

Hashim, M., Ahmad S., Johari, M.A., Pour, A.B., 2013. Automatic lineaments extraction in a heavily vegetated region using Landsat Enhanced Thematic Mapper (ETM+) imagery. Advances in space research. 51. 874-890.

Healy D., Rizzo R.E., Cornwell D.G., Farrell N.J.C., Watkins H., Timms N.E., Gomez-Rivas E., Smith M., 2017. FracPaQ: A MATLAB™ toolbox for the quantification of fracture patterns // Journal of Structural Geology. Vol. 95, February, p. 1-16. https://doi.org/10.1016/j.jsg.2016.12.003

Hoang, N., Flower M.F.J., Chí, C.T., Xuân P.T., Quý H.V., Sơn T.T., 2013. Collision-induced basalt eruptions at Pleiku and BuÔn Mê Thuôt, south-central Viet Nam. Journal of Geodynamics, 69:65–83. http://dx.doi.org/10.1016/j.jog.2012.03.012

Horton R.E., 1945. Erosional development of streams and their drainage basins; hydrophysical approach to quantitative morphology // GSA Bulletin (1945) 56 (3): 275-370.

Jakobsson, et al., 2017. Post-glacial flooding of the Beringia land bridge dated to 11,000 cal yrs BP based on new geophysical and sediment records. Clim. Past Discuss. http://dx.doi.org/10.5194/cp-2017-11, 2017.

Kaydalov, V.A., Novoselov B.A., Maksimova L.B., 2001. State geological map of Russian federation. Scale 1:200000. Second edition. Sheet N-54-XXI. Legend. Saint-Petersburg. 247 p. (in Russian).

Khanchuk, A.I. (editor), 2006. Geodynamics, magmatism and metallogeny of Russian East. Vladivostok, Dal'nauka. 1 &2. 982 pp. (in Russian).

Khanchuk, A.I., 1993. Geological structure and development of the continental framing of northwest Pacific. In: Extended Abstract of Doctoral (geol.-miner.) Dissertation. GIN RAN, Moscow, pp. 1–31 (in Russian).

Khomich, V.G., Boriskina, N.G., 2014a. Localization of PGE mineralization in southeastern Russia. Russ. Geol. Geophys. 55, 842–853. http://dx.doi.org/10.1016/j.rgg.2014.06.004.

Khomich, V.G., Boriskina, N.G., 2014b. Geodinamic settings of formation of large deposits of precious and radioactive elements in Inagli-Konder-Feklistov belt and its flanks. Geology and mineral resources of Siberia, 3s–1, 37–40 (in Russian).

Khomich, V.G., et al, 2017. Characteristics and genesis of the Mnogovershinnoe gold-silver deposit, SE Russia. Ore Geology Reviews (2017), http://dx.doi.org/10.1016/j.oregeorev.2017.01.017

Kiden, P., Törnqvist, T.E., 1998. Can river terrace flights be used to quantify Quaternary tectonic uplift rates? Journal Of Quaternary Science. 1998. 13 (6). P. 573–575.

Krasny, L.I., Volsky A.S., Pan Yun Bao, 1999. Geological map of Priamurye and adjacent areas. Scale 1:2500000. Supporting statement. Saint-Petersburg – Blagoveshchensk – Harbin. 1999. 134 p.

Kumagai Naoichi, Sasajima Sadao, Ito Hidebumi, 1978. Long-term Creep of Rocks: Results with Large Specimens Obtained in about 20 Years and Those with Small Specimens in about 3 Years. // Journal of the Society of Materials Science (Japan). Japan Energy Society. 27 (293): 157–161. https://ci.nii.ac.jp/naid/110002299397/

Lague, D., Crave, A., Davy P., 2003. Laboratory experiments simulating the geomorphic response to tectonic uplift. Journal Of Geophysical Research, Vol. 108, No. B1. P. 3-1–3-20.

Lave J., Avouac J.P., 2001. Fluvial incision and tectonic uplift across the Himalaya of Central Nepal. Journal of geophysical research. Vol. 106. No. B11. P. 26561-26591.

Maruyama, S., Santosh, M., Zhao, D., 2007. Superplume, supercontinent, and postperovskite: mantle dynamics and antiplate tectonics on the Core-Mantle Boundary. Gondwana Res. 11, 7–37. http://dx.doi.org/10.1016/j.gr.2006.06.003.

Miller, M.S., Becker, W.T., 2014. Reactivated lithospheric-scale discontinuities localize dynamic uplift of the Moroccan Atlas Mountains. Geology 42, P. 35-38.

Okada, Y., 1985. Surface deformation due to shear and tensile faults in a half-space. Bulletin of the Seismological Society of America. Vol. 75. No. 4, Pp. 1135-1154.

Park, S.-C., Yoo, D.-G., Lee, C.-W., and Lee, E.-I. 2000. Last glacial sea-level changes and paleogeography of the Korea (Tsushima) Strait. Geo-Marine Letters 20: 64–71

Peltier A., Beauducel F., Villeneuve N., Ferrazzini V., Di Muro A., Aiuppa A. Derrien A., Jourde K., Taisne B., 2016. Deep fluid transfer evidenced by surface deformation during the 2014–2015 unrest at Piton de la Fournaise volcano. Journal of Volcanology and Geothermal Research. 321 (2016). 140–148. http://dx.doi.org/10.1016/j.jvolgeores.2016.04.031.

Petryschevsky, A.M., 1984. Tectonics of Lower Amur region. Russian journal of Pacific geology. Vol .1. 1984. P. 62-67. (in Russian).

Philosophov, V.P., 1967. About meaning of orders of valleys and watershed lines in geologic-geographic researches / V.P. Philosophov // Tasks of morphometry. Vol. 2. Saratov. SSU. 1967, pp. 4-67. (in Russian).

Philosophov, V.P., 1975. Principals of morphometric method tectonic structures search / Saratov. SSU. 232 p. (in Russian).

Schofield, J.C., 1964. Postglacial sea levels and isostatic uplift. New Zealand Journal of Geology and Geophysics 7(2):359-360. https://doi.org/10.1080/00288306.1964.10420182

Shevyrev, S.L. Algorithmization of remote sensing analysis of structural and substantial parageneses of gold-bearing regions (Mnogovershinnoe field, Khabarovsk krai) / Proceedings of VSU. Geology. 2017. Vol. 2. pp 115-121. (in Russian).

Shevyrev, S.L., 2018. LEFA. Lineament extraction and fracture analysis software. Official web site. URL: http://lefa.geologov.net

Siddall, M., Rohling, E.J., Almogi-Labin, A., Hemleben, Ch., Meischner, D., Schmelzer, I., Smeed, D.A., 2003. Sea-level fluctuations during the last glacial cycle. Nature 423, 853–858.

Sillitoe, R.H., 2010. Porphyry copper systems. Economic geology. V. 105. №1. P.3-41.

Smith, D.E., Barlow N.L.M., Bradley S.L., Firth C.R., Hall A.M., Jordan J.T., Long D., 2017. Quaternary sea level change in Scotland. Earth and Environmental Science Transactions of the Royal Society of Edinburgh. P. 1–38.

Stockamp J., Bishop P., Li Zh., Petrie E.J. , Hansom J. Rennie A., 2016. State-of-the-art in studies of glacial isostatic adjustment for the British Isles: a literature review. Earth and Environmental Science Transactions of the Royal Society of Edinburgh 106(3):1-26.

Strahler, A. N., 1957. Quantitative analysis of watershed geomorphology / A.N. Strahler // Eos Trans. AGU. Vol. 38(6), p. 913-920.

Šujan M., Rybár S., 2014. The development of Pleistocene river terraces in the eastern part of the Danube Basin. Acta Geologica Slovaca 6(2). P. 107-122.

Tarı U., Tüysüz O., Blackwell B.A.B., Mahmudd Z., Florentin J.A., Qid J., Gença Ş.C., Skinner A.R., 2018 Sealevel change and tectonic uplift from dated marine terraces along the eastern Mediterranean coast, southeastern Turkey. Palaeogeography, Palaeoclimatology, Palaeoecology. https://doi.org/10.1016/j.palaeo.2018.07.003

Tikhonov, I.N., Lomtev, V.L., 2014. Shallow-focus seismicity of Okhotsk sea and its probable tectonic nature. Questions of engineering seismology. 2014. Vol. 41. №1. P. 25.

Trasatti, E., Marra, F., Polcari, M., Etiope, G., Ciotoli, G., Darrah, T. H., Tedesco D., Stramondo S., Florindo F., Ventura G., 2018. Coeval uplift and subsidence reveal magma recharging near Rome (Italy). Geochemistry, Geophysics, Geosystems, 19. https://doi.org/10.1029/2017GC007303

Turcotte, D. L., Schubert, G., 2014. Geodynamics. Cambridge University Press. Third edition. 2014. − P. 657.

Utkin, V.P., 1999. Horst-accretionary systems, rift-grabens and volcano-plutonic belts of the Russian Far East south. Paper 2. Volcano-plutonic belts: structuralcompositional characteristics and regularities of formation. Russ. J. Pac. Geol. 14, 891–922.

Van der Hilst, R. D., Widiyantoro, S., Engdahl, E. R. Evidence for deep mantle circulation from global tomography. Nature 386, 578–584 (1997).

Van Wijk, J., Koning, D., Axen, G., Coblentz, D., Gragg, E., Sion, B., 2018. Tectonic subsidence, geoid analysis, and the Miocene-Pliocene unconformity in the Rio Grande rift, southwestern United States: Implications for mantle upwelling as a driving force for rift opening. Geosphere. 14 (2). https://doi.org/10.1130/GES01522.1

Weil-Accardo, J. et al, 2016 Two hundred thirty years of relative sea level changes due to climate and megathrust tectonics recorded in coral microatolls of Martinique (French West Indies). Journal of Geophysical Research: Solid Earth. 121(4).

Zhang, H.F., Li, S.R., Santosh, M., Liu, J.J., DiWu, C.R., Zhang, H., 2013. Magmatism and metallogeny associated with mantle upwelling: zircon U–Pb and Lu–Hf constraints from the gold-mineralized Jinchang granite, NE China. Ore Geol. Rev. 54, 138–156

Zhao, D., Pirajno, F., Dobretsov, N.L., Liu, L., 2010. Mantle structure and dynamics under East Russia and adjacent regions. Russ. Geol. Geophys. 51, 925–938. http://dx.doi.org/10.1016/j.rgg.2010.08.003.

Figure Captions

Fig. 1. Schematic map of the Bekchiul massif and adjacent area. The map is a compilation of Kochanova, Aronson (1969; 1970), Kaydalov, Roganov (2013), and Fat'yanov, Khomich (1997).

Fig. 2. Outcrop of the Paleogene montzonite dike intruding cretaceous volcanic rock.

Fig. 3. Geological map of the Mnogovershinnoe ore field showing an erosion cut of the ore zones (author of the photo, Dr. Prof. V.G. Khomich).

Fig. 4. Ore textures in the vein metasomatic zones of the Mnogovershinnoe deposit. A – Striped adularia quartz ore with fragments of early fine-grained quartz (Q). Ore body of Verkhnee. B – Striped adularia quartz ore with a fragment of siltstone (black). Ore body of Verkhnee. C-D – Wollastonite (Woll) and bustamite (Bust) substitutes carbonates (Carb). Sphalerite and galena are confined to the contact and are distributed along the margins. Ore zone of Promezhutochnaya. E – Sulfide pyrite chalcopyrite ore. Ore body Severnoe. F – Fragment of the striped adularia quartz ore in the dike of the basalt porphyrite (Porph). Ore body Verkhnee (Khomich et al., 2017).

Fig. 5. Relationships between different stages of mineralization in the Mnogovershinnoe deposit. A – Zonal magnesian-ferruginous metasomatite. Diop – diopside, Ep + Act – epidote and actinolite, Py – pyrite, Neph – nephritis, Tre – tremolite; B – Q – quartz, Tell – tellurides, Py – pyrite; C – Dol – hydrothermal dolomite, Mt – magnetite; D – Bust + Rod – bustamite and rhodonite, Q – quartz;

E – Q + Bust + Rod – quartz, bustamite and rhodonite; F – Q + Woll – quartz and wollastonite (Khomich et al., 2017).

Fig. 6. Stages and mineral associations of the Mnogovershinnoe deposit (after Khomich et al., 2017 with minor amendments).

Fig. 7. Drilling cross-section of Tyvlinka-Sivuk interfluve that depicts a position of the eroded Miocene weathering crust (pebbles with blue clay). After Temnikov M.S and Sosnin A.I. (Kaydalov et al., 2001) with changes.

Fig. 8. Stream order map of the Mnogovershinnoe deposit area and surroundings.

Fig. 9. Juxtaposition of base erosional surfaces of the second (BLS2) and third (BLS3) order streams and surface difference (BLDS23).

Fig. 10. Maps showing base erosional surfaces of the (a) second- and (b) third-order streams and (c) their difference surface.

Fig. 11. Lineaments overlaying the Landsat 8 band 7 mosaicing images for the Bekchiul massif and its surroundings.

Fig. 12. Result of the semiquantitative model implementation to hypothesize the Bekchiul massif's core isostatic uplift. Model parameters: dynamic viscosity of the core block and media, $\nu_b = \nu_m = 4.5e19$ Pa·s; density of the core block, $\rho_b=2.65$ g/cm^3; and density of the media, $\rho_m=2.60$ g/cm^3.

Fig. 13. Tectonic interpretation of the base surfaces difference map compared to faults

Fig. 14 Evolution of the Bekchiul volcanic-plutonic center and relief forming processes. Radiometric dates of stages 4-5, 8 were taken from (*Kaydalov et al., 2001*), using the K-Ar method. The remaining stages are established after (Khomich et al., 2017) with K-Ar dating by IGEM RAS with amendments.

Figure Captions

Fig. 1. Schematic map of the Bekchiul massif and adjacent area. The map is a compilation of Kochanova, Aronson (1969; 1970), Kaydalov, Roganov (2013), and Fat'yanov, Khomich (1997).

Fig. 2. Outcrop of the Paleogene montzonite dike intruding cretaceous volcanic rock.

Fig. 3. Geological map of the Mnogovershinnoe ore field showing an erosion cut of the ore zones (author of the photo, Dr. Prof. V.G. Khomich).

Fig. 4. Ore textures in the vein metasomatic zones of the Mnogovershinnoe deposit. A – Striped adularia quartz ore with fragments of early fine-grained quartz (Q). Ore body of Verkhnee. B – Striped adularia quartz ore with a fragment of siltstone (black). Ore body of Verkhnee. C-D – Wollastonite (Woll) and bustamite (Bust) substitutes carbonates (Carb). Sphalerite and galena are confined to the contact and are distributed along the margins. Ore zone of Promezhutochnaya. E – Sulfide pyrite chalcopyrite ore. Ore body Severnoe. F – Fragment of the striped adularia quartz ore in the dike of the basalt porphyrite (Porph). Ore body Verkhnee (Khomich et al., 2017).

Fig. 5. Relationships between different stages of mineralization in the Mnogovershinnoe deposit. A – Zonal magnesian-ferruginous metasomatite. Diop – diopside, Ep + Act – epidote and actinolite, Py – pyrite, Neph – nephritis, Tre – tremolite; B – Q – quartz, Tell – tellurides, Py – pyrite; C – Dol – hydrothermal dolomite, Mt – magnetite; D – Bust + Rod – bustamite and rhodonite, Q – quartz; E – Q + Bust + Rod – quartz, bustamite and rhodonite; F – Q + Woll – quartz and wollastonite (Khomich et al., 2017).

Fig. 6. Stages and mineral associations of the Mnogovershinnoe deposit (after Khomich et al., 2017 with minor amendments).

Fig. 7. Drilling cross-section of Tyvlinka-Sivuk interfluve that depicts a position of the eroded Miocene weathering crust (pebbles with blue clay). After Temnikov M.S and Sosnin A.I. (Kaydalov et al., 2001) with changes.

Fig. 8. Stream order map of the Mnogovershinnoe deposit area and surroundings.

Fig. 9. Juxtaposition of base erosional surfaces of the second (BLS2) and third (BLS3) order streams and surface difference (BLDS23).

Fig. 10. Maps showing base erosional surfaces of the (a) second- and (b) third-order streams and (c) their difference surface.

Fig. 11. Lineaments overlaying the Landsat 8 band 7 mosaicing images for the Bekchiul massif and its surroundings.

Fig. 12. Result of the semiquantitative model implementation to hypothesize the Bekchiul massif's core isostatic uplift. Model parameters: dynamic viscosity of the core block and media, $\nu_b = \nu_m = 4.5e19$ Pa·s; density of the core block, $\rho_b=2.65$ g/cm^3; and density of the media, $\rho_m=2.60$ g/cm^3.

Fig. 13. Tectonic interpretation of the base surfaces difference map compared to faults

Fig. 14 Evolution of the Bekchiul volcanic-plutonic center and relief forming processes. Radiometric dates of stages 4-5, 8 were taken from (*Kaydalov et al., 2001*), using the K-Ar method. The remaining stages are established after (Khomich et al., 2017) with K-Ar dating by IGEM RAS with amendments.

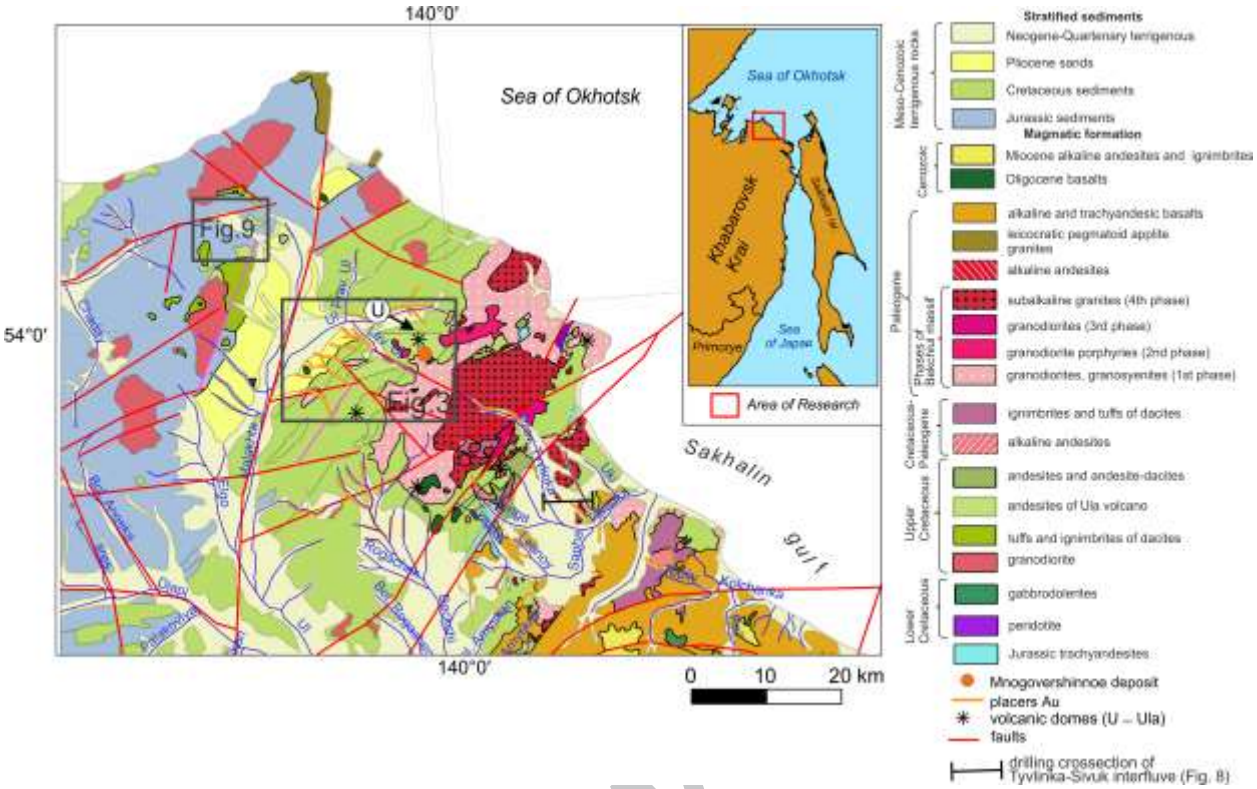
140°0'
54°0'
Sea of Okhotsk
Fig.9
Fig.3
U
Sakhalin
gulf
Sea of Okhotsk
Khabarovsk Krai
Primorye
Sea of Japan
Area of Research
0 10 20 km
Stratified sediments
Meso-Cenozoic terrigenous rocks
Neogene-Quarternary terrigenous
Pliocene sands
Cretaceous sediments
Jurassic sediments
Magmatic formation
Cenozoic
Miocene alkaline andesites and ignimbrites
Oligocene basalts
Paleogene
Plutons of Bikinsky massif
alkaline and trachyandesitic basalts
leucocratic pegmatoid aplite granites
alkaline andesites
subalkaline granites (4th phase)
granodiorites (3rd phase)
granodiorite porphyries (2nd phase)
granodiorites, granosyenites (1st phase)
Cretaceous-Paleogene
ignimbrites and tuffs of dacites
alkaline andesites
Upper Cretaceous
andesites and andesite-dacites
andesites of Ula volcano
tuffs and ignimbrites of dacites
granodiorite
Lower Cretaceous
gabbrodolerites
peridotite
Jurassic trachyandesites
Mnogovershinnoe deposit
placers Au
volcanic domes (U – Ula)
faults
drilling crosssection of Tyvlinka-Sivuk interfluve (Fig. 8)


SW
NE
Paleogene montzodiorite dike
Cretaceous volcanic rocks
intrusive contact
Slope deposits

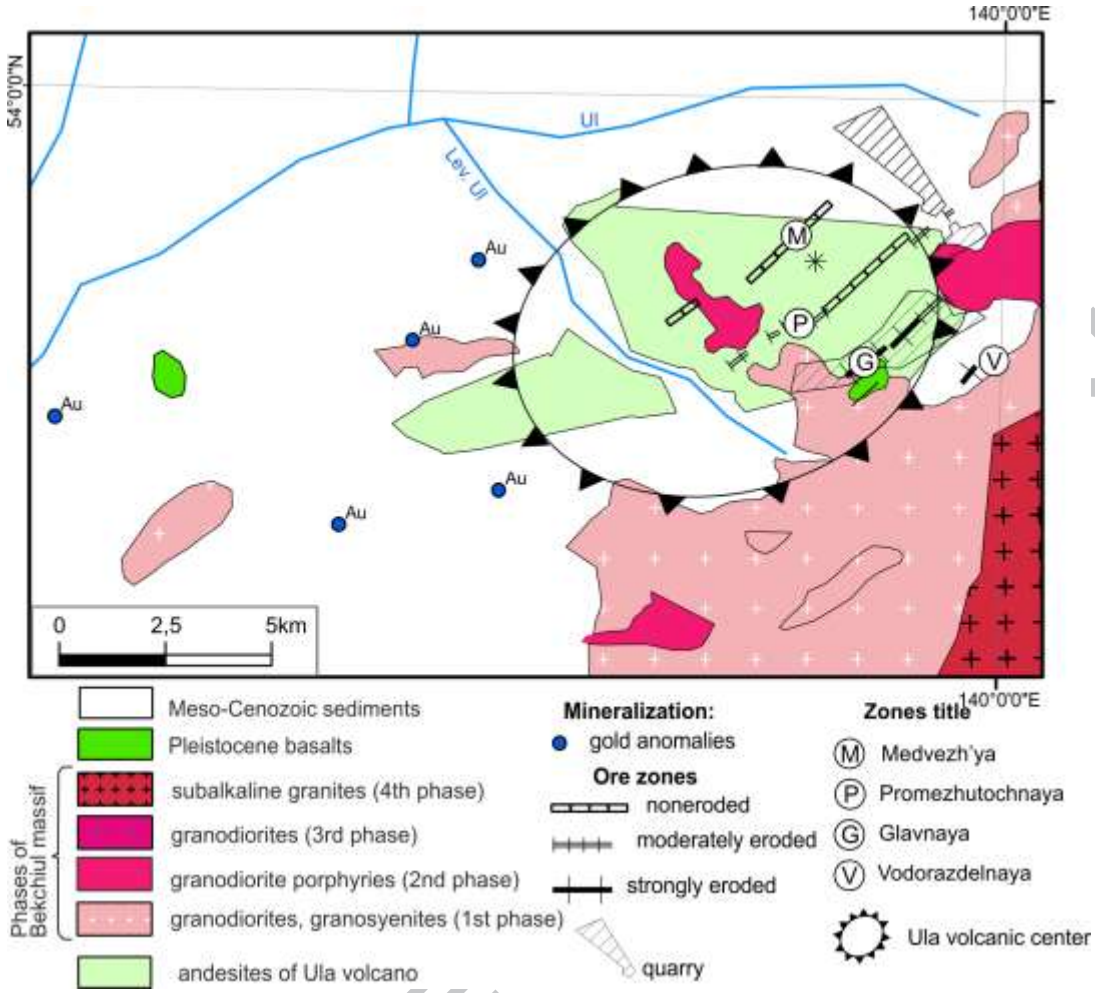


A
Q
Q
Q
Q
B
C
Carb
Woll
D
Carb
Bust
Carb
E
Py
Chpy
F
Porph

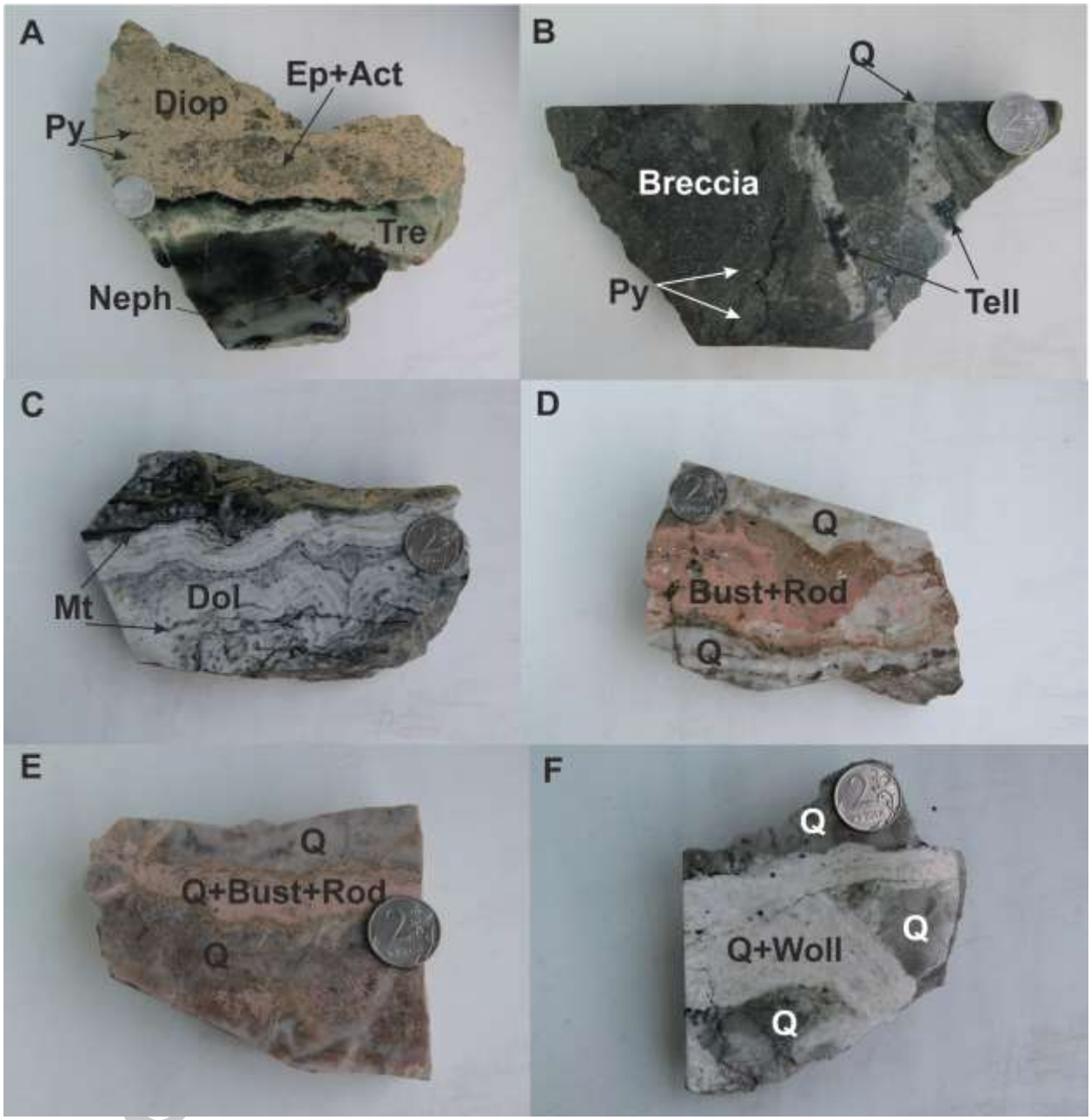
A
Diop
Ep+Act
Py
Tre
Neph
B
Q
Breccia
Py
Tell
C
Mt
Dol
D
Q
Bust+Rod
Q
E
Q
Q+Bust+Rod
Q
F
Q
Q
Q+Woll
Q

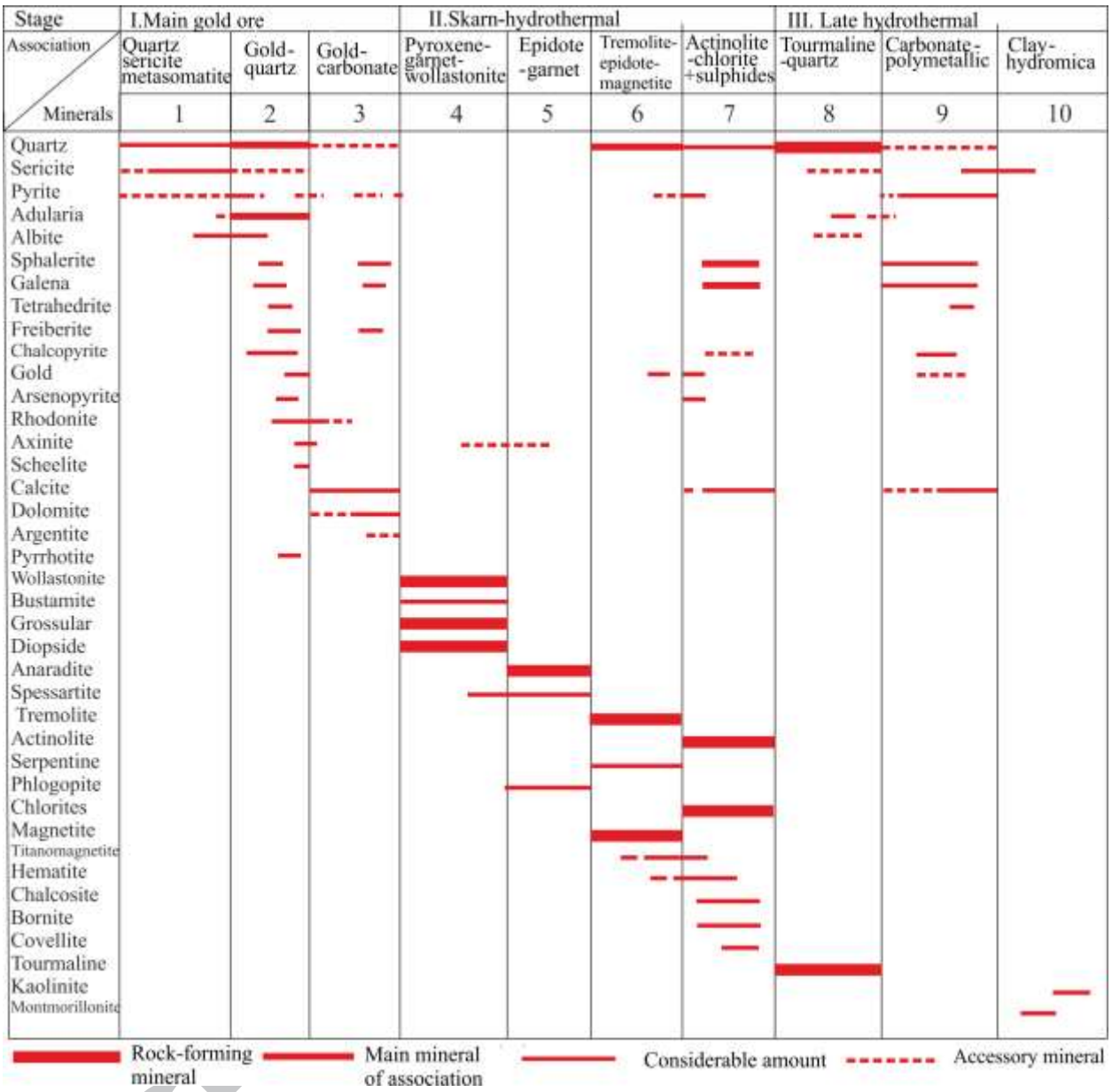

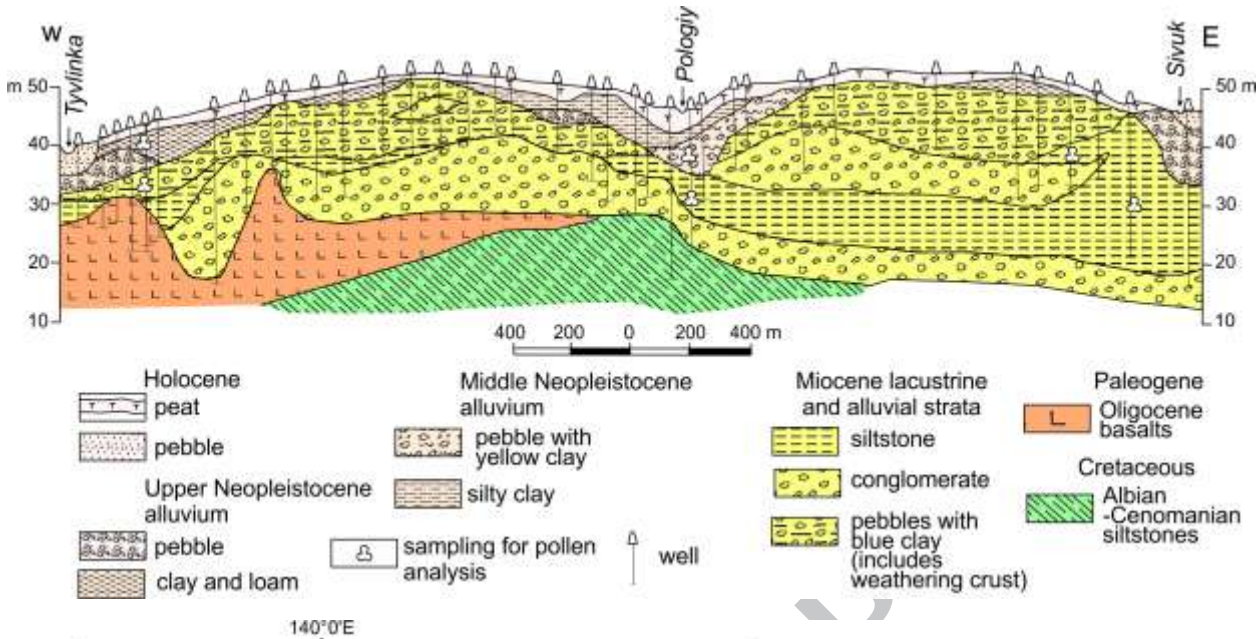
W
E
Tyvlinka
Pologiy
Sivuk
m 50
40
30
20
10
50 m
400 200 0 200 400 m
Holocene
peat
pebble
Upper Neopleistocene alluvium
pebble
clay and loam
Middle Neopleistocene alluvium
pebble with yellow clay
silty clay
sampling for pollen analysis
well
Miocene lacustrine and alluvial strata
siltstone
conglomerate
pebbles with blue clay (includes weathering crust)
Paleogene
Oligocene basalts
Cretaceous
Albian -Cenomanian siltstones

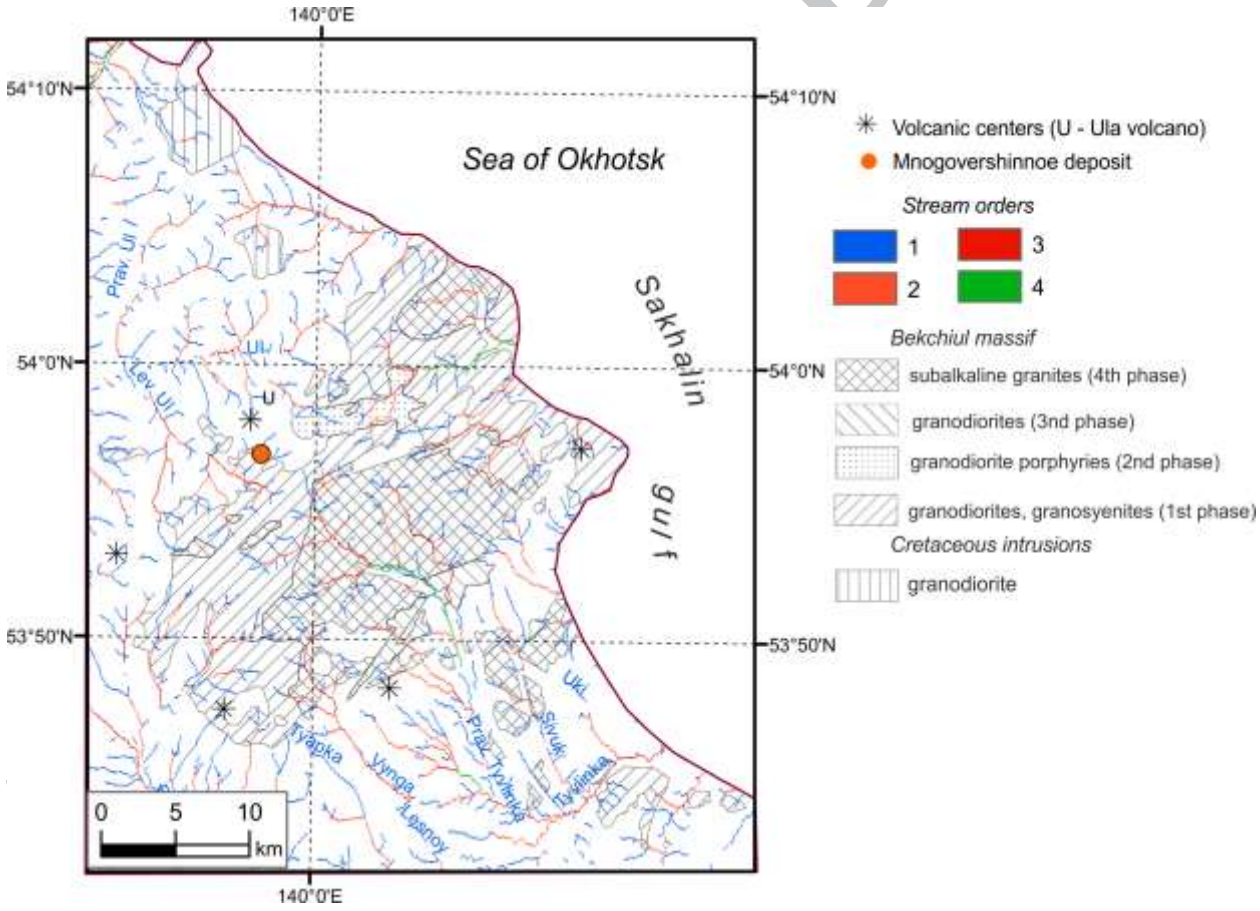
140°0'E
54°10'N
54°0'N
53°50'N
Sea of Okhotsk
Sakhalin
gulf
Prav. Ul
Lev. Ul
Ulu
U
Ukl.
Tyapka
Vynga
Lesnoy
Prav. Tyvlinka
Sivuk
Tyvlinka
0 5 10 km
Volcanic centers (U - Ula volcano)
Mnogovershinnoe deposit
Stream orders
1
2
3
4
Bekchiul massif
subalkaline granites (4th phase)
granodiorites (3nd phase)
granodiorite porphyries (2nd phase)
granodiorites, granosyenites (1st phase)
Cretaceous intrusions
granodiorite

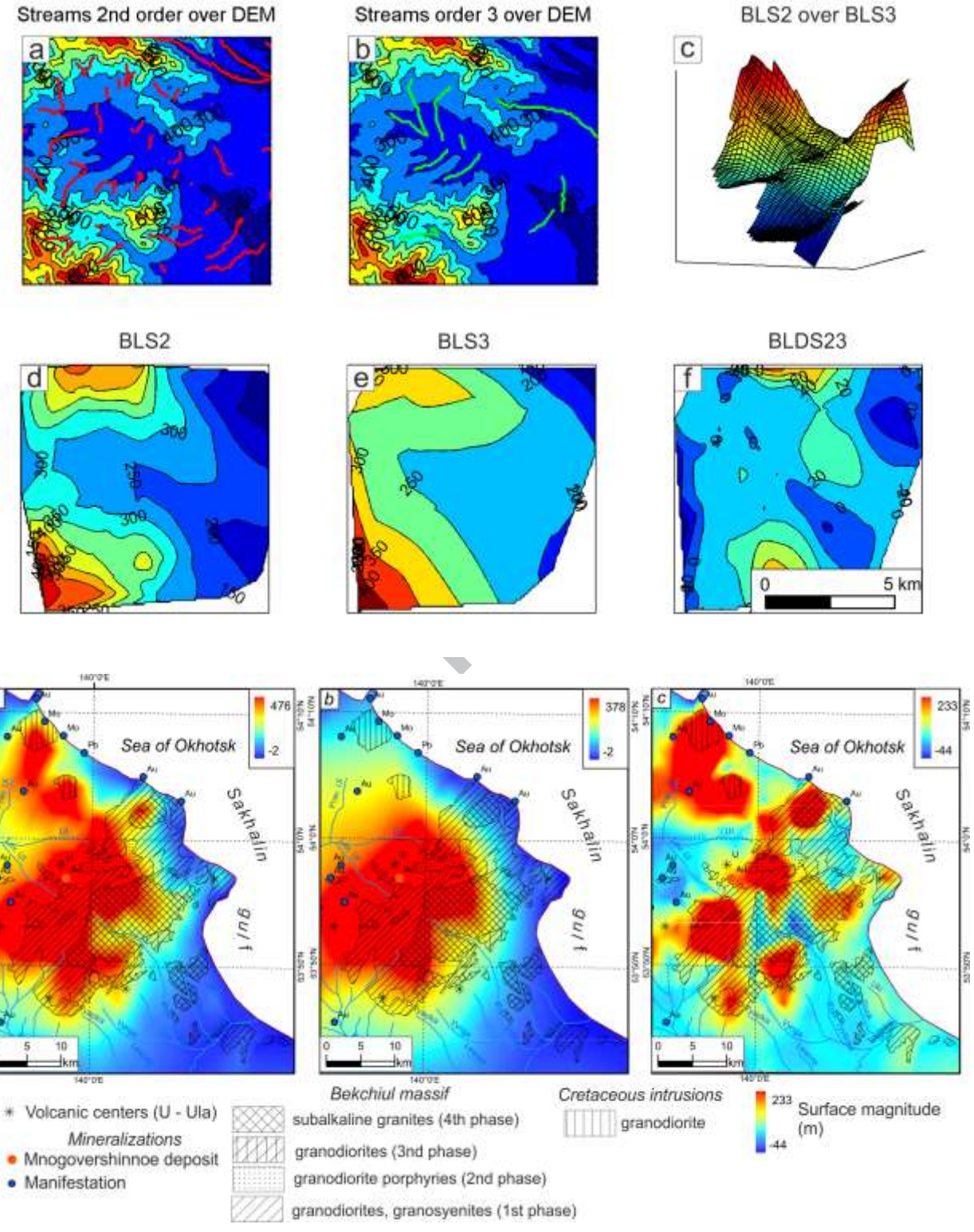
Streams 2nd order over DEM
Streams order 3 over DEM
BLS2 over BLS3
a
b
c
BLS2
BLS3
BLDS23
d
e
f
0
5 km
Sea of Okhotsk
Sakhalin
gulf
476
-2
378
233
-44
0 5 10 km
Volcanic centers (U - Ula)
Mineralizations
Mnogovershinnoe deposit
Manifestation
Bekchiul massif
subalkaline granites (4th phase)
granodiorites (3nd phase)
granodiorite porphyries (2nd phase)
granodiorites, granosyenites (1st phase)
Cretaceous intrusions
granodiorite
Surface magnitude (m)

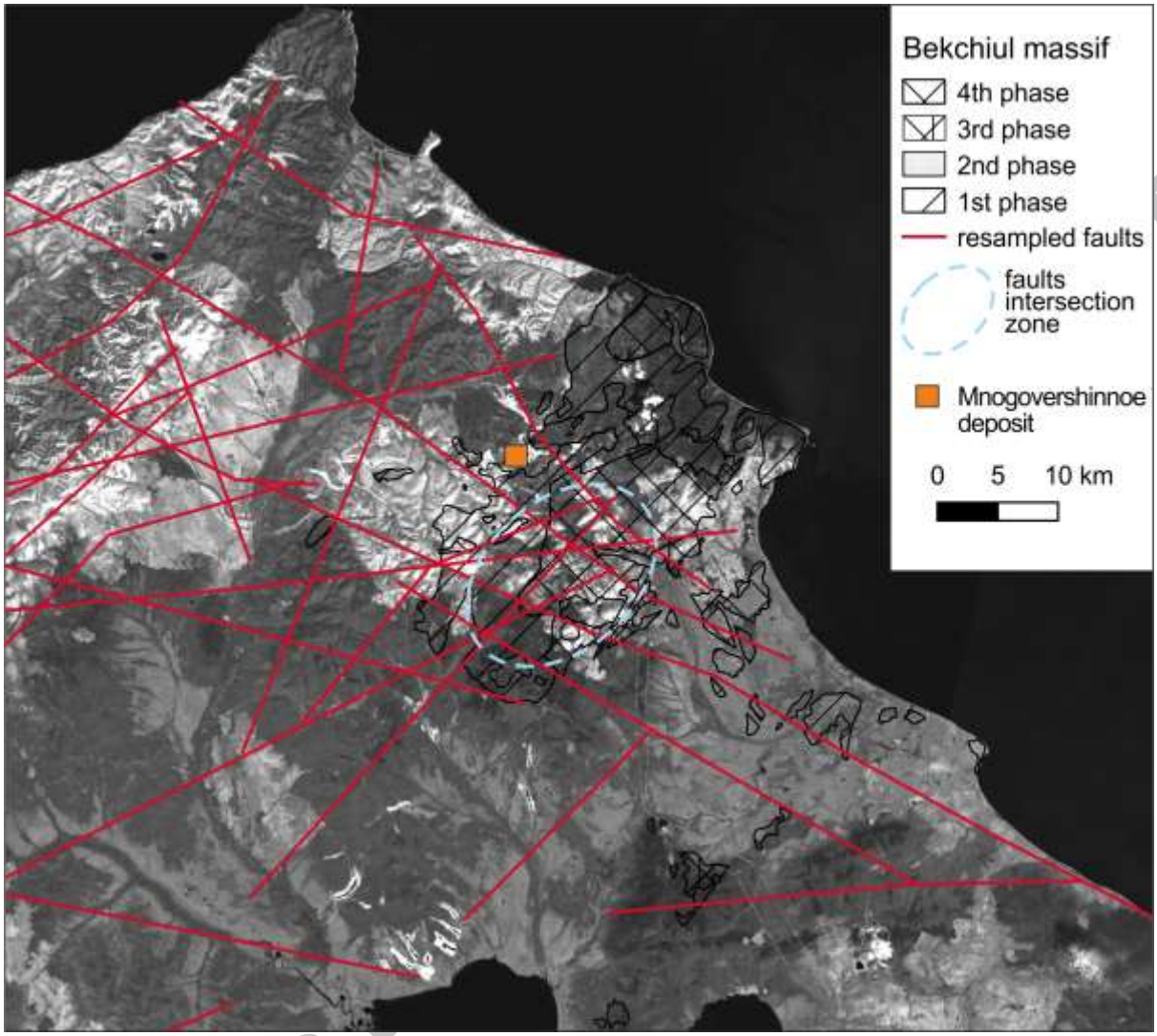

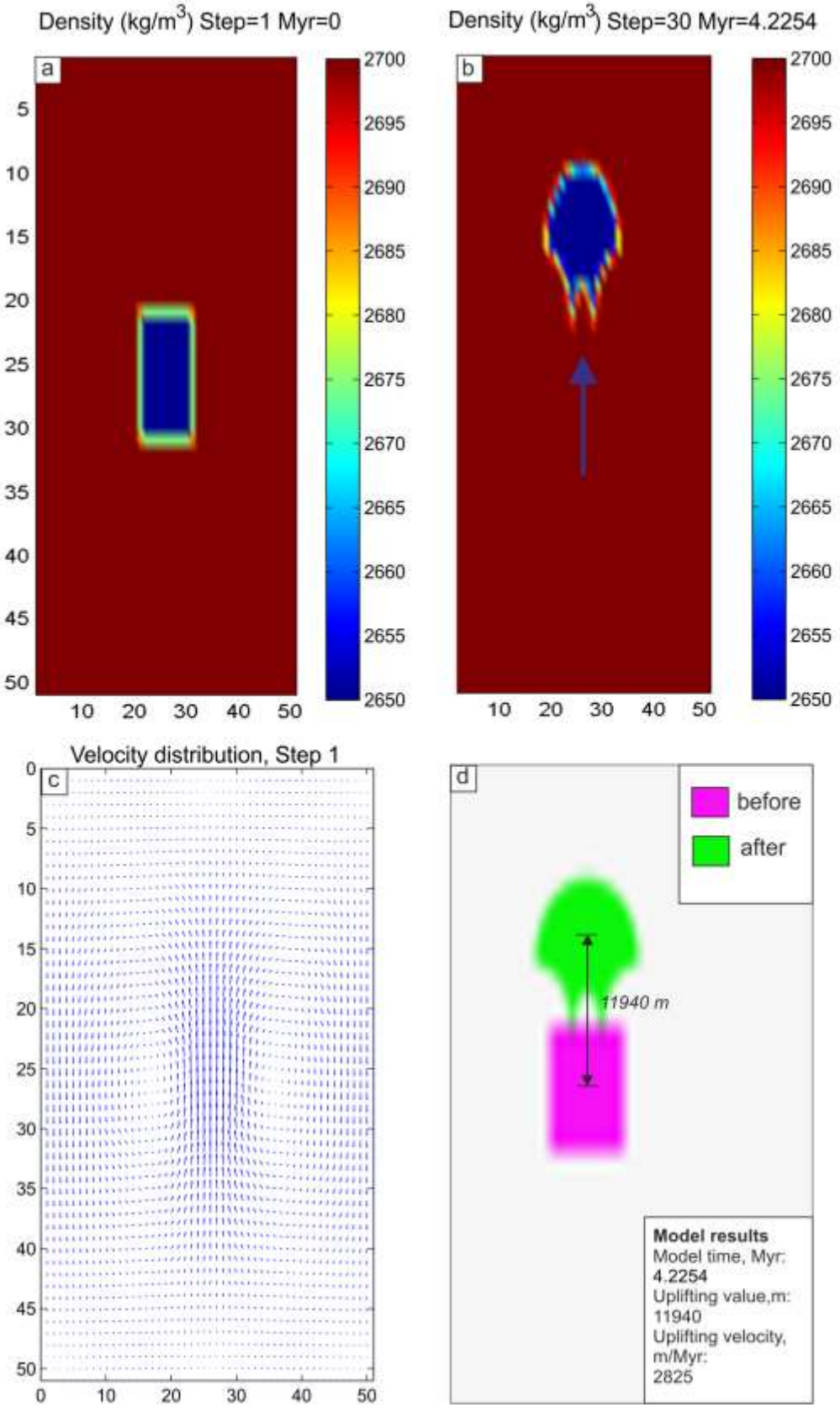
Density (kg/m3) Step=1 Myr=0
a
Density (kg/m3) Step=30 Myr=4.2254
b
2700
2695
2690
2685
2680
2675
2670
2665
2660
2655
2650
Velocity distribution, Step 1
c
d
before
after
11940 m
Model results
Model time, Myr:
4.2254
Uplifting value,m:
11940
Uplifting velocity,
m/Myr:
2825

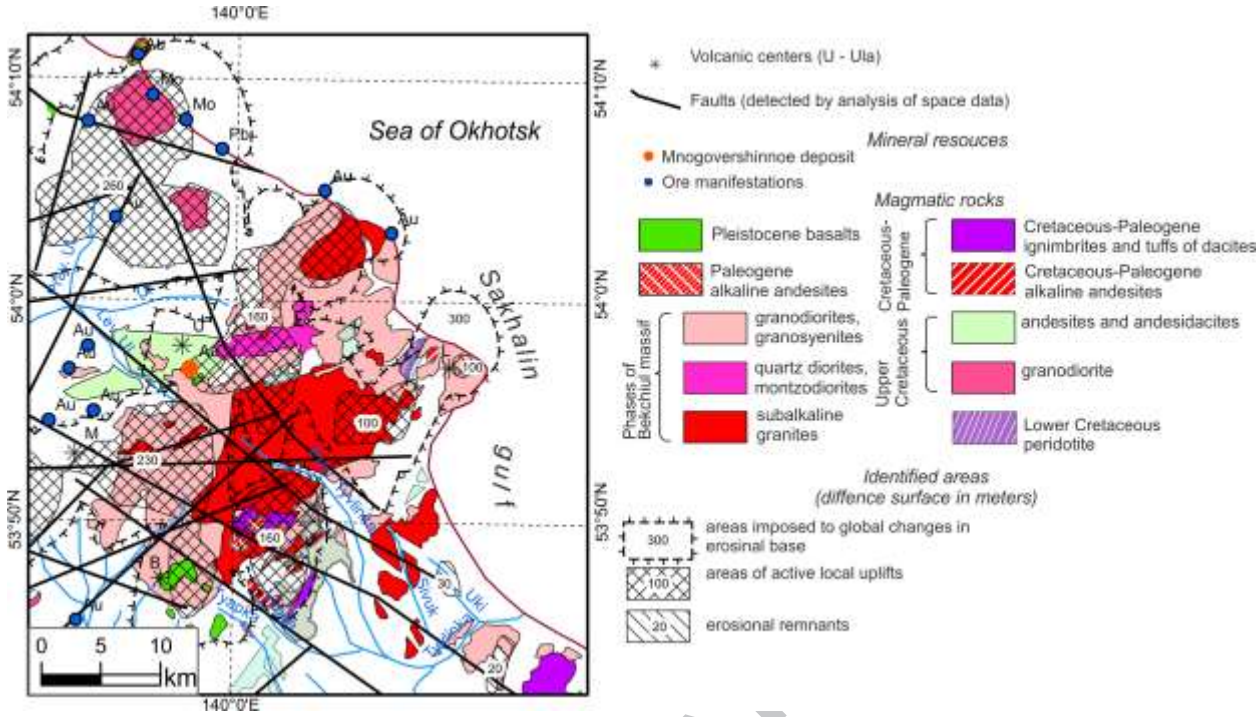

Period	Absolute age, Ma	Stage scheme	Fracture extension: magmatic	Fracture extension: tectonic	Stage description
	0.017	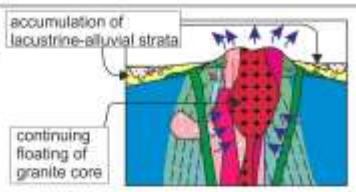			8. Erosion pre-existing rocks; accumulation of continental strata (Miocene); Forming of weathering crust over the Miocene deposits (Pre-Middle Pleistocene); transgressions and regressions (Upper Pleistocene-Holocene); massif's core isostatic floating without thermal field.
Paleogene	24.5	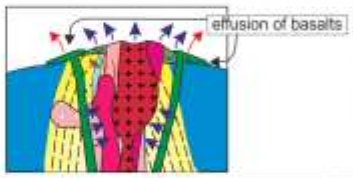			7. Effusion of Oligocene basalts (24.5±2.0 Ma).
		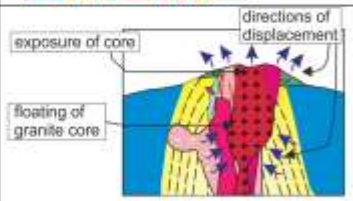			6. Gravitational floating of granite core. Erosion of Bekchiul structure and exposure of subalkaline granite core. Floating core formed marginal uplifts and system of radial faults.
	40	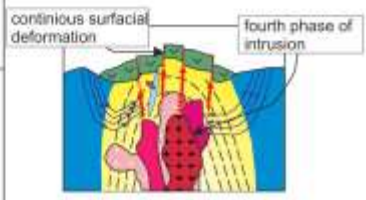			5. Fourth phase intrusion of the subalkaline granites (40 Ma).
	55	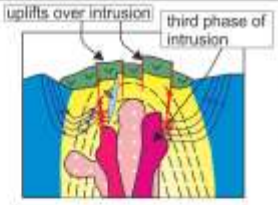			4. Intrusion of the third phase, granodiorites (55 Ma).
	57.3	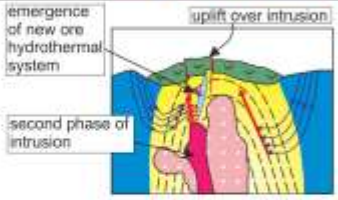			3. Intrusion of the second phase, granodiorite porphyries (57.3±3.0; 57.3±2.6 Ma).
	64.9	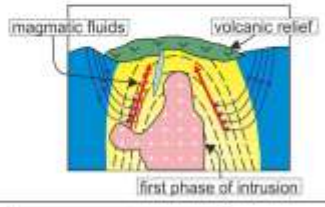			2. Intrusion of granodiorites and granosienites, first phase (75.5±3; 68.3±2.5; 64.9±3 Ma) and andesic volcanism (71.3±3.5; 68.6±3.2 Ma) of Bekchi volcano. Forming of vein metasomatic zones by magmatogenic fluids.
Cretaceous	68.3 68.6 71.3 75.5				
Pre-Upper Cretaceous	>75.5	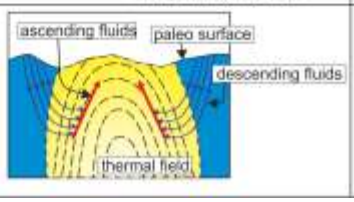			1.Forming of thermal field. Heating of and ascending of descending infiltrating fluids

Table 1. Late Cenozoic events affected vicinity of Bekchiul volcano-magmatic center in Post-Oligocene history

Number	Age, kyr	Age name	Event	Evidences
1	16.5-8	Holocene	Present-time transgression	Recent marine, alluvial and lacustrine sediments of the area
2	16.5-26.5	Upper Pleistocene	Sartan glacial regression	Reduction of the sea and erosion levels up to 120 m, erosion of land alluvial deposits, alluvial deposition on the shelf
3	26.5-37.5	Upper Pleistocene	2nd stage, Kazantsev transgression	Clay and sand of sea terrace
4	38.1-41.3	Upper Pleistocene	1st stage, Karginskoye transgression	First sea terrace and alluvial sea terrace, sands and aleurite
5	60–74	Upper Pleistocene	Zyryan regression	Reduction of the sea and erosion levels up to 120 m, erosion of land alluvial deposits, alluvial deposition on the shelf
6	?	Pre-Middle Pleistocene	Forming of weathering crust	Forming of weathering crust over the Miocene lacustrine-alluvial deposits
7	?	Miocene	Forming of ancient river network	Erosion of Mesozoic sedimentary rocks and Oligocene basalts; accumulation of continental strata

Highlights

- The tectonic position of Mnogovershinnoe gold-silver deposit (Khabarovsk Krai, Russian Far East) is firstly studied in detail using neotectonic reconstruction by base erosional surface analysis.

- Comparison between value of erosion cut and Okhotsk sea regression in the Neo-Pleistocene revealed active uplifting of Bekchiul massif.

- Zones of anomalous differences between base erosion surfaces, obtained for second and third orders of streams reflect position of uplifted peripheral zones of Bekchiul massif and Oligocene volcanic centers.

- Numeric model for isostatic buoyant floating of the massif quartz core corresponds to actual values of rise in the Neo-Pleistocene.